The Astrophysical Journal, 882:170 (8pp), 2019 September 10 https://doi.org/10.3847/1538-4357/ab384e

A New Model for Electron-capture Supernovae in Galactic Chemical Evolution

Samuel Jones[1], Benoit Côté[2,3,4], Friedrich K. Röpke[5,6], and Shinya Wanajo[7,8,9]
[1] X Computational Physics (XCP) Division and Center for Theoretical Astrophysics (CTA), Los Alamos National Laboratory, Los Alamos, NM 87545, USA
swjones@lanl.gov
[2] Konkoly Observatory, Research Centre for Astronomy and Earth Sciences, Hungarian Academy of Sciences, Konkoly Thege Miklos ut 15-17, H-1121 Budapest, Hungary
[3] National Superconducting Cyclotron Laboratory, Michigan State University, East Lansing, MI 48824, USA
[4] Joint Institute for Nuclear Astrophysics—Center for the Evolution of the Elements, USA
[5] Institut für Theoretische Astrophysik, Zentrum für Astronomie der Universität Heidelberg, Philosophenweg 12, D-69120 Heidelberg, Germany
[6] Heidelberg Institute for Theoretical Studies, Schloss-Wolfsbrunnenweg 35, D-69118 Heidelberg, Germany
[7] Max Planck Institute for Gravitational Physics (Albert Einstein Institute), Am Mühlenberg 1, Potsdam-Golm, D-14476, Germany
[8] Department of Engineering and Applied Sciences, Sophia University, Chiyoda-ku, Tokyo 102-8554, Japan
[9] iTHEMS Research Group, RIKEN, Wako, Saitama 351-0198, Japan
Received 2019 June 6; revised 2019 July 30; accepted 2019 August 1; published 2019 September 16

Abstract

We examine the contribution of electron-capture supernovae (ECSNe), low-mass SNe from collapsing Fe cores (FeCCSNe), and rotating massive stars to the chemical composition of the Galaxy. Our model includes contributions to chemical evolution from both thermonuclear ECSNe (tECSNe) and gravitational collapse ECSNe (cECSNe). We show that if ECSNe are predominantly gravitational collapse SNe but about 15% are partial thermonuclear explosions, the model is able to reproduce the solar abundances of several important and problematic isotopes including ^{48}Ca, ^{50}Ti, and ^{54}Cr together with ^{58}Fe, ^{64}Ni, ^{82}Se, and ^{86}Kr and several of the Zn–Zr isotopes. A model in which no cECSNe occur, only tECSNe with low-mass FeCCSNe or rotating massive stars, proves also very successful at reproducing the solar abundances for these isotopes. Despite the small mass range for the progenitors of ECSNe and low-mass FeCCSNe, the large production factors suffice for the solar inventory of the above isotopes. Our model is compelling because it introduces no new tensions with the solar abundance distribution for a Milky Way model—only tending to improve the model predictions for several isotopes. The proposed astrophysical production model thus provides a natural and elegant way to explain one of the last uncharted territories on the periodic table of astrophysical element production.

Key words: nuclear reactions, nucleosynthesis, abundances – stars: evolution – Sun: abundances – supernovae: general

1. Introduction

Recent progress in observations (Abbott et al. 2017) and modeling (Cowan et al. 2019) lend strong support to neutron star (NS) mergers as the main astrophysical site of the *r* process. Its counterpart neutron-capture processes—the weak and main *s* processes, operating in massive and AGB stars (Busso et al. 1999; Käppeler et al. 2011), respectively—produce familiar abundance patterns that have been studied for several decades now with quite some rigor. The production of the lighter elements (He–Fe) in AGB and massive stars (Herwig 2005; Nomoto et al. 2013), and in thermonuclear and core-collapse supernovae (Woosley et al. 2002; Seitenzahl et al. 2013) have also been extensively studied.

Although our picture of the astrophysical production of nuclear species improves, the origins of a number of isotopes still remain a mystery. One of the remaining blemishes on these nuclear charts are the neutron-rich isotopes ^{48}Ca, ^{50}Ti, ^{54}Cr and isotopes of the elements in the Zn–Zr region. Their production requires special conditions that are reached in explosive thermonuclear burning in high-density material in which electron-captures produce a low Y_e (Meyer et al. 1996). This has been discussed by Woosley (1997) in the context of thermonuclear explosion of very high density carbon/oxygen white dwarfs (CO WDs); however, stellar evolution theory does not support the existence of such objects.

The required nucleosynthetic conditions can, however, be reached in so-called electron-capture supernovae (ECSNe) in massive degenerate oxygen neon (ONe) cores that form in the final evolutionary stages of stars in the mass range of about 8–10 $M_\odot$, in-between AGB stars and massive stars (Nomoto 1984, 1987). For these, two explosion scenarios are discussed: a collapse into an NS (cECSN; Wanajo et al. 2011) and a (partial) thermonuclear disruption (tECSN; Jones et al. 2016) leaving behind an ONeFe WD remnant. Though recent attempts have been made to predict which explosion occurs in nature (Jones et al. 2019; Leung et al. 2019), there remain outstanding uncertainties that make it extremely challenging. It should also be noted that a recent chemical evolution study (Prantzos et al. 2018) demonstrates that the weak *s* process in rotating massive stars (Limongi & Chieffi 2018) can be the predominant source of the elements in the Zn–Zr region.

Here, we present an argument that the thermonuclear explosion channel indeed occurs in nature, probably at a low rate, and is primarily responsible for the solar inventory of ^{48}Ca, ^{50}Ti, and ^{54}Cr and provides a substantial contribution to ^{58}Fe, ^{64}Ni, and ^{66,68}Zn. We show that this model avoids inconsistencies in the production factors of other isotopes. We further develop our model to include some fraction of ECSNe that collapse into NSs and combine the ECSN yields with those from low-mass Fe-core explosions (FeCCSNe, Wanajo et al. 2018) or rotating massive stars (Limongi & Chieffi 2018).

2. Galactic Chemical Evolution (GCE) Models

2.1. Code Description and Ingredients

To bring the nucleosynthesis yields into a galactic context, we use the open-source two-zone chemical evolution model OMEGA+ (Côté et al. 2018). The adopted Milky Way setup is described in Côté et al. (2019)[10] and allows us to reproduce a variety of observational constraints including the current star formation rate, gas inflow rate, star-to-gas mass ratio, and core-collapse and Type Ia supernova rates (CCSN, SNIa). We use mass- and metallicity-dependent yields for both low- and intermediate-mass stars (Cristallo et al. 2015) and for massive stars (Limongi & Chieffi 2018, either rotating or nonrotating models). For each stellar population formed throughout the GCE calculations, we fold the yields with the initial mass function of Kroupa (2001). We use the delayed-detonation N100 model of Seitenzahl et al. (2013) for the yields of SNe Ia, and distribute them within each stellar population following a delay-time distribution (DTD) function in the form of t^{-1} (Maoz et al. 2014, see Ritter et al. 2018 for implementation details). In total, we generate $\sim 10^{-2}$ and $\sim 10^{-3}$ CCSN and SNIa per unit of stellar mass ($M_{\odot}$) formed, respectively.

2.2. Inclusion of ECSNe in the GCE Model

We have considered two sources of yields for ECSNe: those by Jones et al. (2019) for tECSNe and those by Wanajo et al. (2013) for cECSNe, with ejecta masses of 0.95 $M_{\odot}$ and 0.011 $M_{\odot}$ respectively. The abundance distributions for the two yield sets are compared in Figure 1.

The population synthesis calculations in Jones et al. (2019) based on models from Ruiter et al. (2019) suggest that the most common evolutionary channel producing ECSNe is from stars evolving directly toward explosion in binary systems (2.8% of CCSN rate), as opposed to accreting ONe WDs (so-called accretion-induced collapse, AIC, 0.36% of CCSN rate) or isolated single SAGB stars (0.15%). However, it is not clear whether this is the case at all metallicities (Doherty et al. 2015, and references therein). Further population synthesis studies would be highly desirable, in which the underlying assumptions and models are updated and based on the most recent single and binary star models (Tauris et al. 2015; Poelarends et al. 2017; Siess & Lebreuilly 2018).

There are hence two assumptions one could make for the ECSN DTD that bracket the range of possible DTDs: the SAGB channel DTD would be CCSN-like (i.e., with the stellar lifetimes and no further time delay), and the AIC channel would follow more of a single-degenerate SN Ia DTD. We assume that the DTD for stars evolving directly to an ECSN in a binary will be similar to the CCSN-like DTD because no accretion phenomena are involved.

The event rate and integrated number of events as a function of time in the GCE simulations is shown in Figure 2. The red (green) bands show these quantities for ECSNe assuming a CCSN-like (AIC-like) DTD. The AIC DTD was constructed based on the results of Ruiter et al. (2009). In this study the red (CCSN-like) band was used. The lower limit is at 0.5% of the CCSN rate, and the upper limit is at 5% of the CCSN rate. These limits represent the range of ECSN rates that we use for this work. A tECSN rate that is no more than 0.5% of the CCSN rate is needed to reproduce all of the solar ^{48}Ca for a CCSN-like DTD, which increases to 0.7% for and AIC-like DTD.

[10] https://github.com/becot85/JINAPyCEE/blob/master/DOC/OMEGA%2B_Milky_Way_model.ipynb

3. Results

3.1. Thermonuclear ECSNe as the Origin of ^{48}Ca, ^{50}Ti, ^{54}Cr, ^{58}Fe, ^{64}Ni, and ^{66,68}Zn

In this section we demonstrate that tECSNe are able to account for the solar inventory of ^{48}Ca and several other neutron-rich isotopes without introducing new tensions.

In Figure 3 we plot the composition of our Milky Way models relative to the solar composition at the time when the Sun forms. Figure 3(a) shows our fiducial model in which no ECSNe or rotating massive stars were included at all. We note the underproduction of ^{48}Ca, ^{50}Ti, and ^{54}Cr and several isotopes in the Zn–Zr region. We also note at this time that ^{62}Ni is already overproduced in our fiducial model by more than a factor of two. This comes from the *s* process yields we are using (Limongi & Chieffi 2018).

If one attempts to explain the solar ^{48}Ca with cECSNe, one would not only need a much higher ECSN rate than is expected (∼65%), but at such a high rate many of the light trans-Fe isotopes would be overproduced by up to an order of magnitude (Figure 1). Furthermore, the large ratio of ^{48}Ca to both ^{50}Ti and ^{54}Cr in cECSNe is not compatible with the solar abundances. Therefore if all ECSNe collapse into NSs, an additional source of these isotopes would be required.

A model where tECSNe (cECSNe) have been assumed to occur at 0.5% (4.5%) of the CCSN rate with a CCSN-like DTD on top of our fiducial model is shown in Figure 3(b). The addition of tECSNe affects only ^{48}Ca, ^{50}Ti, ^{54}Cr, ^{58}Fe, ^{64}Ni, and ^{66,68}Zn, and all of these isotopes match the solar abundances better when tECSN yields are included, with the former three being the most markedly improved. The rate estimate of 0.5% (0.7%) of the CCSN rate for the CCSN-like (AIC-like) DTD is similar to but lower than the simpler estimate by Jones et al. (2019).

We note that while the model in Figure 3(b) reproduces well the solar abundance of ^{48}Ca, ^{50}Ti, and ^{54}Cr, ^{50}Ti and ^{54}Cr are now slightly overproduced in the best-fit model for ^{48}Ca (though within a factor of two). The Y_e of ^{48}Ca is 0.417 and that of ^{50}Ti is 0.44, this hints at ^{48}Ca being produced in slightly higher density conditions, or at least lower Y_e. There are still uncertainties in the hydrodynamic tECSN simulations that could therefore affect the ^{48}Ca/^{50}Ti ratio in the ejecta. For example, the ratio is sensitive to the weak reaction rates used in the nucleosynthesis calculations (Jones et al. 2019). Moreover, the ratio is greater than unity in the bound remnants, indicating that if slightly more of the lower Y_e material were ejected the ^{48}Ca/^{50}Ti ratio might better match the solar one. If the expansion timescale of the WD as the deflagration burns through it were slightly longer, the simulation might also result in a more favorable ^{48}Ca/^{50}Ti ratio. This uncertainty is related to not knowing the precise ignition conditions of the ONe core (central density and initial ignition geometry).

3.2. A New Model for GCE

In this section we present models in which different combinations of tECSNe, cECSNe, and low-mass FeCCSNe occur. We demonstrate that such models—in particular one where all three types of SNe occur—are quite successful at

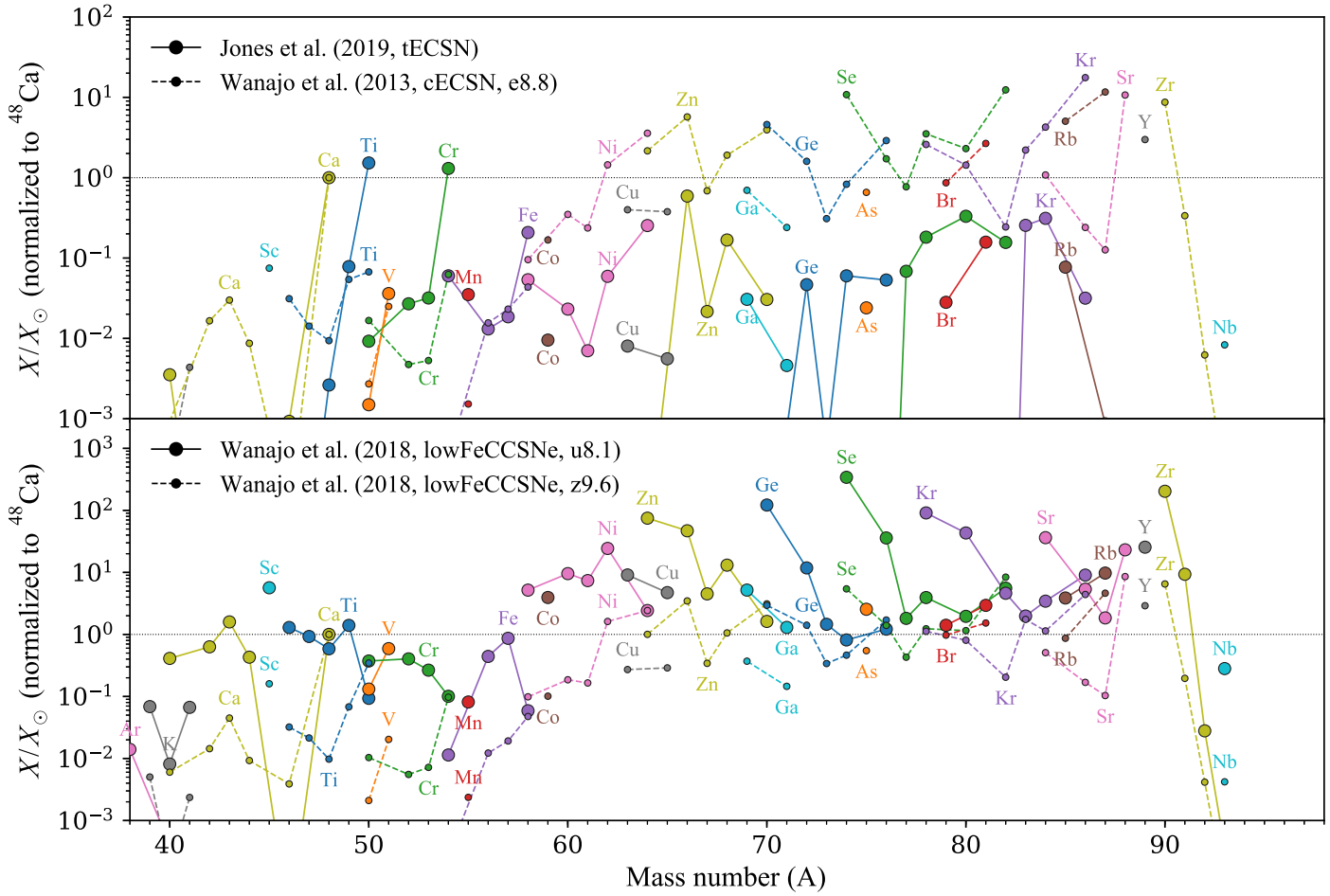

Figure 1. Top panel: comparison of ejected compositions from the thermonuclear ECSN model of Jones et al. (2019, solid lines) and the gravitational collapse e8.8 ECSN model of Wanajo et al. (2013, dashed lines). Bottom panel: comparison of ejected compositions from the u8.1 (solid lines) and z9.6 (dashed lines) low-mass FeCCSN models of Wanajo et al. (2018). All compositions have first been normalized to the solar isotopic composition, and then renormalized to shift ^{48}Ca to 1.0 by dividing by the overproduction factor of ^{48}Ca, $X_{\rm ejected}(^{48}{\rm Ca})/{\rm X}_{\odot}(^{48}{\rm Ca})$. The overproduction factors for ^{48}Ca were 19, 0.40, and 19 for e8.8, u8.1, and z9.6, respectively. The equivalent value for the G14a tECSN model from Jones et al. (2019) is 1.40×10^4 without an envelope, or 1.58×10^3 if one were to assume that the progenitor was an 8.8 $M_{\odot}$ star.

reproducing the solar composition when applied in a GCE code, especially for several challenging isotopes.

3.2.1. The Role of TECSNe

The models all assume a CCSN-like DTD for ECSNe with tECSNe occurring at 0.5% of the CCSN rate in order to match the solar abundance of ^{48}Ca by the time the Sun forms. It is only by the inclusion of tECSNe that the ^{48}Ca, ^{50}Ti, and ^{54}Cr abundances are simultaneously and satisfactorily explained (as discussed in Section 3.1).

3.2.2. cECSN Compliment

As Wanajo et al. (2011) have shown, cECSNe are a promising site for production of the problematic region Zn–Zr (Figure 1), which is underproduced when we include tECSNe at the necessary rate to match ^{48}Ca. Additionally, the diluted H/He envelopes of cECSNe do not contribute many isotopes below $A = 48$, either. cECSNe therefore provide quite a good compliment to tECSNe and together exhibit performance favorable to only including one or the other. Indeed, when we include cECSNe at 4.5% of the CCSN rate in addition to tECSNe at 0.5% of the CCSN rate (Figure 3(b)), the whole picture looks much improved over the case where no ECSNe are included (Figure 3(a)).

One might imagine that if the tECSN ejecta would reach only slightly lower $Y_{\rm e}$, then more Zn–Zr would be produced (e.g., Figure 1 of Jones et al. 2019), the $^{48}{\rm Ca}/^{50}{\rm Ti}$ ratio would fit even better and one may not need cECSNe at all. However, the most neutron-rich isotopes such as ^{82}Se and ^{86}Kr are more naturally fit with cECSNe, which exhibits higher overproduction relative to the more proton-rich isotopes of Se and Kr, than tECSNe.

3.2.3. Low-mass FeCCSNe: Is There a Need for cECSNe at All?

Wanajo et al. (2018) have reported nucleosynthesis calculations based on CCSN simulations for progenitors at the low-mass end of Fe core formation for which the progenitor structure is similar to an ECSN progenitor (i.e., with a steep core-density gradient; see Müller 2016, their Figure 1). The nucleosynthesis is similar to cECSNe although there are some differences (Figure 1), and there is slightly more variety in the progenitor structures. Like ECSNe, these low-mass FeCCSN events are also expected to occur in a relatively narrow mass range (less than 1 $M_{\odot}$, A. Heger 2019, private communication).

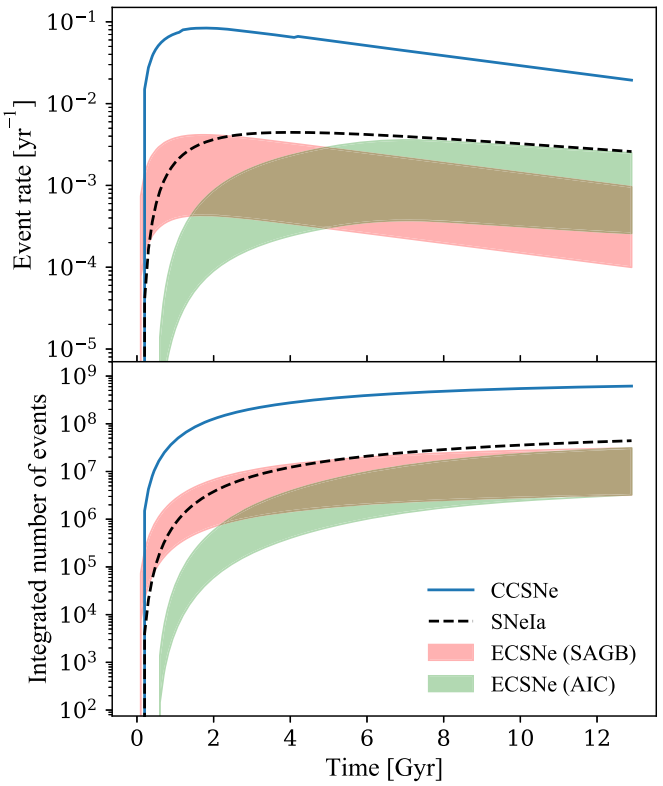

Figure 2. Top panel: rate of SN events over the course of the simulation. We assume the Sun forms after 8.5 Gyr of evolution. Bottom panel: integrated number of SN events. The broad bands show the predicted contribution of ECSNe, assuming the progenitors are single stars (SAGB, red bands) or accreting ONe WDs (AIC, green bands). For the red bands, the lower and upper values correspond to 0.5% and 5% the rate of CCSNe. The former is the rate needed for thermonuclear ECSNe to reproduce the abundance of ^{48}Ca, and the latter is the rate adopted for the contribution of gravitational collapse ECSNe shown in Figure 3(b). Assuming accreting ONe WDs for the progenitors of ECSNe, those rates needed to be increased by 40% in order to recover the same number of ECSNe by the end of the simulations (see the green band in the bottom panel).

Milky Way GCE models mixing only tECSNe and low-mass FeCCSNe with the fiducial model (Figures 3(c) and (d)) were computed, which used the yield from models u8.1 and z9.6 from Wanajo et al. (2018), respectively.[11] The results in panels (b) and (d) look very similar indeed, suggesting that the role of cECSNe in GCE could potentially be superseded by low-mass FeCCSNe. This would be the case if all ECSNe are in fact tECSNe, which is still under debate. We concede, however, that the model in Figure 3(c) performs more poorly for several of the isotopes in the Zn–Zr region. For a good fit when there are no cECSNe, most low-mass FeCCSNe would need to exhibit yields similar to those from the z9.6 model.

Finally, we have constructed a model in which we combine tECSNe, cECSNe, and the two low-mass FeCCSNe (Figure 3(e)). The rates have been tuned by hand to bring a maximum number of isotopes close to the solar composition, within a factor of two. This model is not aimed to be the best-fit model, but rather a proof of concept that ECSNe and low-mass FeCCSNe can be combined together without creating any tension. Conversely to the models with no cECSNe, this model requires that most low-mass FeCCSNe produce yields similar to the u8.1 model. In this model we are able to match the solar abundance distribution to within a factor of approximately two for almost all Zn–Zr isotopes except for ^{84}Sr and ^{96}Zr. We note that neither cECSNe nor low-mass FeCCSNe produce a great deal of isotopes below $A = 48$ because of the very thin C/O shells between the cores and the low-density H/He envelopes of their progenitors. Similarly, the tECSNe models have such high production factors for ^{48}Ca, ^{50}Ti, and ^{54}Cr that when they occur at a rate that reproduces the solar inventory of ^{48}Ca, very little material with $A < 48$ is produced. This is the reason why new tensions are not introduced when including the models, they essentially just fill in some of the missing gaps.

3.2.4. Including Rotating Massive Stars

Figure 4 shows the same chemical evolution models as in Figure 3, but using the rotating models of Limongi & Chieffi (2018) along with the metallicity-dependent mixture of rotation velocities as adopted in Prantzos et al. (2018). Using those models instead of the nonrotating ones required a slight recalibration of our GCE models in terms of gas fraction and gas outflows. To recover a similar fit for ^{48}Ca, we increased the tECSN rate from 0.5% to 0.6%. But the rates for cECSNe and low-mass FeCCSNe are the same as those in Figure 3.

Because of the neutron-capture elements produced in the rotating models of Limongi & Chieffi (2018), the addition of cECSNe and low-mass FeCCSNe only improves the predictions for a limited number of isotopes compared to when using the nonrotating models. But our predictions still demonstrate that cECSNe and low-mass FeCCSNe could occur individually at a rate between about 1%–10% the rate of regular CCSNe without introducing any tension, besides possibly ^{70}Zn (see panels (b) and (d) of Figure 4). In particular, those are needed in our models to improve the predictions for ^{64}Zn, ^{80,82}Se, ^{84}Kr, and the *p*-process isotope ^{74}Se. In any case, tECSNe are still needed to reproduce ^{48}Ca, ^{50}Ti, and ^{54}Cr all together.

Our predictions for the fiducial models with stellar rotation are similar to the ones presented in Prantzos et al. (2018) from Si to Zn. However, we predict an underproduction of ^{50}Ti and ^{54}Cr compared to the latter study. This is because we used the delayed-detonation N100 model of Seitenzahl et al. (2013) for Type Ia supernovae while Prantzos et al. (2018) used the W7 model of Iwamoto et al. (1999), which results from a one-dimensional simulation. This geometry implies that the ashes remain at the stellar center for an artificially long period of time being exposed to high densities. Consequently, neutronization by electron-capture reactions is increased. In contrast, the three-dimensional N100 model self-consistently includes buoyancy effects, which quickly drive burned material to low-density regions. Moreover, the W7 yields of Iwamoto et al. (1999) do not yet account for the revised electron-capture rates of Langanke & Martínez-Pinedo (2000) and thus overestimate the production of ^{50}Ti and ^{54}Cr (Brachwitz et al. 2000). For the neutron-capture elements, the differences likely come from the fact that we did not include the *r* process in our calculations in order to leave room for ECSNe and low-mass FeCCSNe. We note that using rotating models solved the overproduction predicted for ^{62}Ni.

[11] The progenitor models of e8.8 (Miyaji & Nomoto 1987; Nomoto 1987), u8.1, and z9.6 (unpublished; an extension of Heger & Woosley 2010) are those with zero-age main-sequence masses (and initial metallicity) of 8.8 $M_\odot$ (1 $Z_\odot$), 8.1 $M_\odot$ (10^{-4} $Z_\odot$), and 9.6 $M_\odot$ (0 $Z_\odot$), respectively. The models u8.1 and z9.6 are at the low-mass ends of CCSN progenitors with the adopted metallicities; the latter exhibits slightly steeper core-density gradient (Müller 2016). Note that all relevant isotopes (^{48}Ca and heavier) are made in the innermost region of exploding material, in which the initial metallicity has no effect (high temperature and weak interaction reset the abundance distribution).

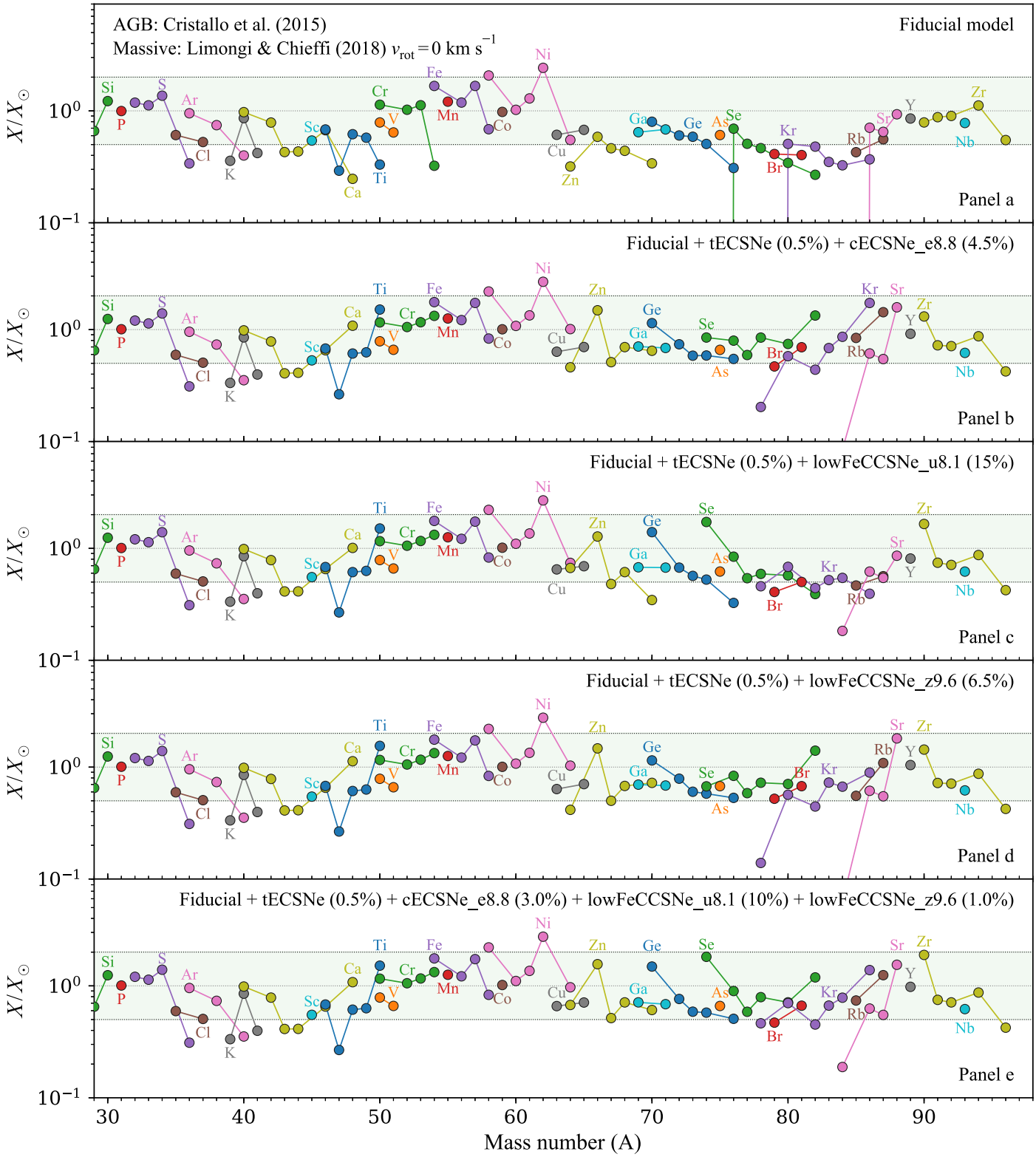

Figure 3. Galaxy model composition relative to solar when the Sun forms. Panel (a): fiducial model without ECSN and low-mass Fe CCSN (low-FeCCSNe). Panel (b): predictions assuming a combination of thermonuclear SNe (tECSNe) and gravitational collapse ECSNe (cECSNe). Panel (c): combination of tECSNe and lowFeCCSNe (u8.1). Panel (d): combination of tECSNe and lowFeCCSNe (z9.6). Panel (e): combination of tECSNe, cECSNe, and lowFeCCSNe (u8.1 and z9.6). The percentages in parenthesis in the panel legend represent the rate of the considered site in percentage of the CCSN rate. Panels (b) through (e) show three additional isotopes (^{74}Se, ^{78}Kr, and ^{84}Sr, which are *p*-isotopes) compared to the fiducial prediction shown in Panel (a). Those isotopes are not present in the yields of Cristallo et al. (2015) and Limongi & Chieffi (2018).

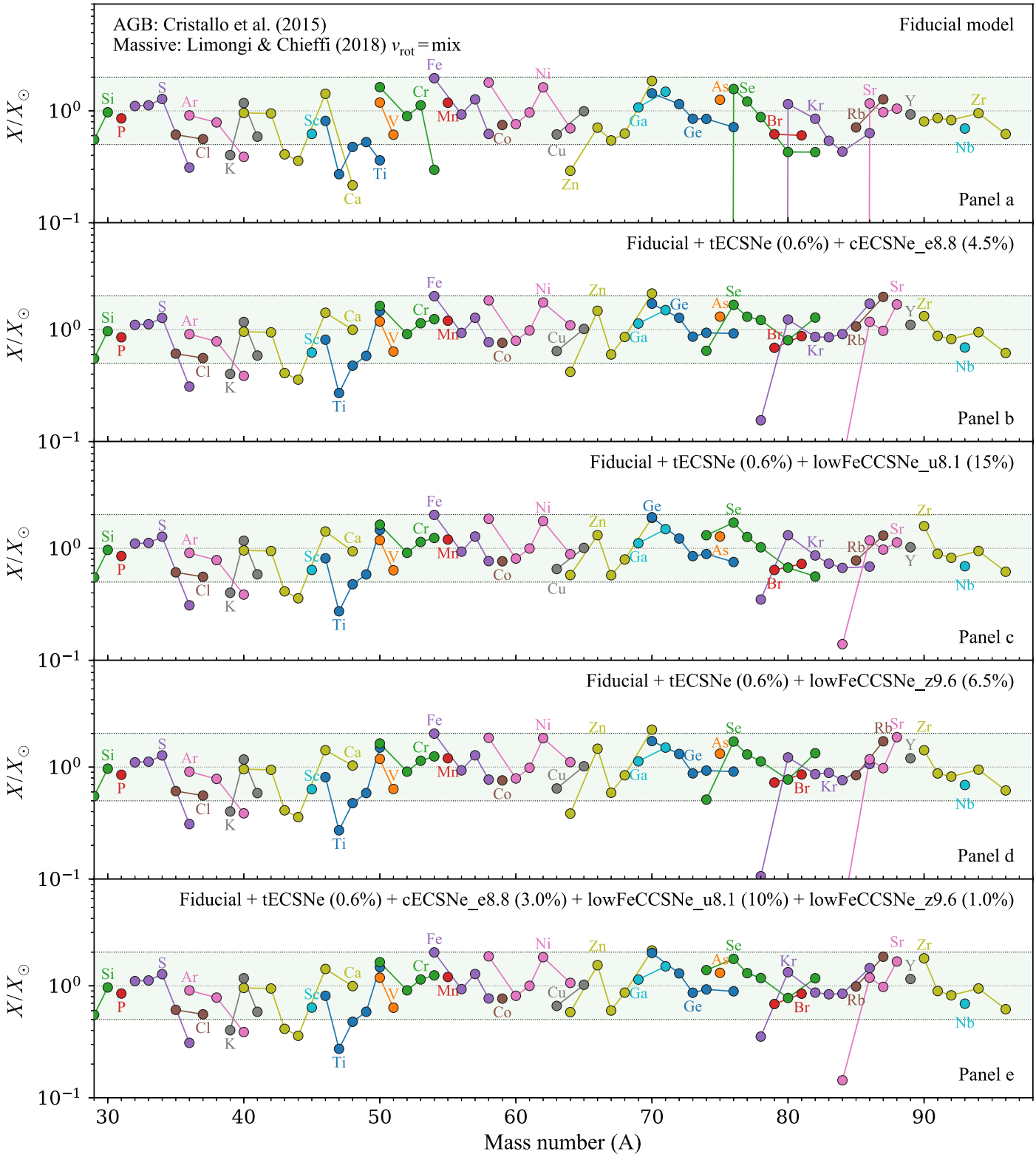

Figure 4. Same as Figure 3, but using the rotating massive star models of Limongi & Chieffi (2018). We adopted the same metallicity-dependent mix of rotation velocities as presented in Figure 4 of Prantzos et al. (2018). The tECSNe rate has been increased to 0.6% to recover the abundance of ^{48}Ca, while all other rates were kept as in Figure 3.

4. Interpretation of Results

We have demonstrated that assuming both partial thermonuclear explosion and gravitational collapse into an NS are outcomes of ECSNe that are realized in nature, GCE models of the Milky Way are more universally successful for the solar inventory several isotopes including ^{48}Ca, ^{50}Ti, ^{54}Cr, and Zn–Zr. We have also shown, however, that models where all ECSNe are thermonuclear explosions are also very successful

when yields from low-mass FeCCSNe and/or rotating massive stars are included.

Our combined model required all three types of SNe to occur, and that tECSNe (cECSNe) occur at 0.5% (3.0%) of the CCSN rate, and low-mass FeCCSNe occur at 11%. This model improves the agreement with the solar abundance distribution without introducing significant new tensions. In this section we discuss what the implications of such models are in a broader astrophysical context.

4.1. Compatibility of Rate Estimates

How do the assumed rates compare with other rate estimates? Single star models (Poelarends 2007; Poelarends et al. 2008; Doherty et al. 2015) typically predict a range of rates for ECSNe in the range of 1%–20% of the CCSN rate. Population synthesis simulations estimate ∼3% (Jones et al. 2019), with the majority coming from binary systems but not accreting ONe WDs. Our rate for ECSNe (3.5%–5.0%) is compatible with both these estimates when one considers the outstanding uncertainties (Jones et al. 2016; Leung et al. 2019).

4.2. Implications for ECSNe

Since the border between gravitational collapse and thermonuclear explosion is very sensitive to the progenitor and deflagration ignition conditions, it may well be that some ONe core stars collapse and others explode. This requires some variety in either the progenitors or the ignition conditions, which one might perhaps expect if $A = 24$ electron-capture reactions drive convective motions in the core (Schwab et al. 2017).

In the model we have proposed, about 85% of ECSNe would still produce a low-mass NS with a low kick velocity. This means that many of the phenomena attributed to ECSNe (BeX systems with low orbital eccentricity, low kick NS populations) could still be explained by invocation of cECSNe as their origin.

If all ECSNe were tECSNe and left behind bound WD remnants, another explanation for low-mass, low kick NSs must be sought. It is conceivable, however, that low-mass FeCCSNe take over the role of cECSNe completely, in which case all ECSNe events could be thermonuclear explosions. This implies that the lower ECSNe rate of 0.5%–0.7% of the CCSN rate is realized. That rate could be larger if the ejecta masses from tECSNe were smaller than current model predictions.

5. Conclusions and Outlook

We have shown that tECSNe present a compelling explanation for the origin of ^{48}Ca, ^{50}Ti, and ^{54}Cr in the solar system. Moreover, if tECSNe and either of cECSNe or low-mass FeCCSNe occur in nature, GCE models of the Milky Way produce improved results with respect to the solar abundance distribution. We note that there is no other appreciable source known for the isotopes ^{48}Ca, ^{50}Ti, and ^{54}Cr.

Our results add further weight to the argument that tECSNe do occur in nature. This argument is supported by potential observations of their candidate WD remnants (Jones et al. 2019; Raddi et al. 2019) and isotopic ratios in pre-solar grains (Völkening & Papanastassiou 1990; Woosley 1997; Nittler et al. 2018; Jones et al. 2019). Unfortunately, all of the evidence is circumstantial at this point. Looking into the implications of tECSNe for the diffuse galactic ^{60}Fe concentration could provide further constraints.

Including tECSNe into GCE models erases one of the last remaining blemishes in cosmic nucleosynthesis with a viable astrophysical source model. In this work, we have not considered a possible contribution of the *r* process to the Galactic inventory of the Zn–Zr region. Further studies on the progenitor evolution toward ECSNe, rate and explosion mechanism, and an implementation of other possible astrophysical sources are required to substantiate this model.

The authors would like to thank the anonymous referee for their critical reading and constructive feedback and suggestions for this manuscript. The authors acknowledge the Lorentz Center workshop "Electron-capture initiated stellar collapse" at which some of the ideas in this article germinated. The authors also acknowledge support from the ChETEC COST Action (CA16117) and HITS gGmbH. B.C. acknowledges support from the ERC Consolidator Grant (Hungary) funding scheme (Project RADIOSTAR, G.A. n. 724560) and the National Science Foundation (NSF, USA) under grant No. PHY-1430152 (JINA Center for the Evolution of the Elements). This work made use of the Heidelberg Supernova Model Archive (HESMA; Kromer et al. 2017), https://hesma.h-its.org. The work of F.R. is supported by the Klaus Tschira Foundation and by the Collaborative Research Center SFB 881 "The Milky Way System" of the German Research Foundation (DFG). This work was supported by the US Department of Energy LDRD program through the Los Alamos National Laboratory. Los Alamos National Laboratory is operated by Triad National Security, LLC, for the National Nuclear Security Administration of U.S. Department of Energy (Contract No. 89233218NCA000001).

ORCID iDs

Samuel Jones https://orcid.org/0000-0003-3970-1843
Benoit Côté https://orcid.org/0000-0002-9986-8816

References

Abbott, B. P., Abbott, R., Abbott, T. D., et al. 2017, ApJL, 848, L12
Brachwitz, F., Dean, D. J., Hix, W. R., et al. 2000, ApJ, 536, 934
Busso, M., Gallino, R., & Wasserburg, G. J. 1999, ARA&A, 37, 239
Côté, B., Lugaro, M., Reifarth, R., et al. 2019, ApJ, 878, 156
Côté, B., Silvia, D. W., O'Shea, B. W., Smith, B., & Wise, J. H. 2018, ApJ, 859, 67
Cowan, J. J., Sneden, C., Lawler, J. E., et al. 2019, arXiv:1901.01410
Cristallo, S., Straniero, O., Piersanti, L., & Gobrecht, D. 2015, ApJS, 219, 40
Doherty, C. L., Gil-Pons, P., Siess, L., Lattanzio, J. C., & Lau, H. H. B. 2015, MNRAS, 446, 2599
Heger, A., & Woosley, S. E. 2010, ApJ, 724, 341
Herwig, F. 2005, ARA&A, 43, 435
Iwamoto, K., Brachwitz, F., Nomoto, K., et al. 1999, ApJS, 125, 439
Jones, S., Röpke, F. K., Fryer, C., et al. 2019, A&A, 622, A74
Jones, S., Röpke, F. K., Pakmor, R., et al. 2016, A&A, 593, A72
Käppeler, F., Gallino, R., Bisterzo, S., & Aoki, W. 2011, RvMP, 83, 157
Kromer, M., Ohlmann, S., & Röpke, F. K. 2017, MmSAI, 88, 312
Kroupa, P. 2001, MNRAS, 322, 231
Langanke, K., & Martínez-Pinedo, G. 2000, NuPhA, 673, 481
Leung, S.-C., Nomoto, K., & Suzuki, T. 2019, arXiv:1901.11438
Limongi, M., & Chieffi, A. 2018, ApJS, 237, 13
Maoz, D., Mannucci, F., & Nelemans, G. 2014, ARA&A, 52, 107
Meyer, B. S., Krishnan, T. D., & Clayton, D. D. 1996, ApJ, 462, 825
Miyaji, S., & Nomoto, K. 1987, ApJ, 318, 307
Müller, B. 2016, PASA, 33, e048
Nittler, L. R., Alexander, C. M. O'D., Liu, N., & Wang, J. 2018, ApJL, 856, L24

Nomoto, K. 1984, ApJ, 277, 791
Nomoto, K. 1987, ApJ, 322, 206
Nomoto, K., Kobayashi, C., & Tominaga, N. 2013, ARA&A, 51, 457
Poelarends, A. J. T. 2007, PhD thesis, Utrecht Univ.
Poelarends, A. J. T., Herwig, F., Langer, N., & Heger, A. 2008, ApJ, 675, 614
Poelarends, A. J. T., Wurtz, S., Tarka, J., Cole Adams, L., & Hills, S. T. 2017, ApJ, 850, 197
Prantzos, N., Abia, C., Limongi, M., Chieffi, A., & Cristallo, S. 2018, MNRAS, 476, 3432
Raddi, R., Hollands, M. A., Koester, D., et al. 2019, MNRAS, 489, 1489
Ritter, C., Côté, B., Herwig, F., Navarro, J. F., & Fryer, C. L. 2018, ApJS, 237, 42
Ruiter, A. J., Belczynski, K., & Fryer, C. 2009, ApJ, 699, 2026
Ruiter, A. J., Ferrario, L., Belczynski, K., et al. 2019, MNRAS, 484, 698
Schwab, J., Bildsten, L., & Quataert, E. 2017, MNRAS, 472, 3390
Seitenzahl, I. R., Ciaraldi-Schoolmann, F., Röpke, F. K., et al. 2013, MNRAS, 429, 1156
Siess, L., & Lebreuilly, U. 2018, A&A, 614, A99
Tauris, T. M., Langer, N., & Podsiadlowski, P. 2015, MNRAS, 451, 2123
Völkening, J., & Papanastassiou, D. A. 1990, ApJL, 358, L29
Wanajo, S., Janka, H.-T., & Müller, B. 2011, ApJL, 726, L15
Wanajo, S., Janka, H.-T., & Müller, B. 2013, ApJL, 767, L26
Wanajo, S., Müller, B., Janka, H.-T., & Heger, A. 2018, ApJ, 852, 40
Woosley, S. E. 1997, ApJ, 476, 801
Woosley, S. E., Heger, A., & Weaver, T. A. 2002, RvMP, 74, 1015